ACS Catalysis

Research Article

pubs.acs.org/acscatalysis

Enhancement of Dehydrogenation and Hydride Transfer by La^{3+} Cations in Zeolites during Acid Catalyzed Alkane Reactions

Florian Schüßler, Stefan Schallmoser, Hui Shi,[†] Gary L. Haller, Erika Ember, and Johannes A. Lercher*

Department of Chemistry, Catalysis Research Center, Technische Universität München, Lichtenbergstraße 4, 85747 Garching, Germany

ABSTRACT: La^{3+} cations exchanged into ultrastable zeolite Y and zeolite X promote catalytic isomerization, cracking, and alkylation of alkanes. La^{3+} cations stabilize the zeolite lattices and, more importantly, polarize alkane C−H bonds to enhance the rates of all three reactions. This unique activity leads to stable cracking and isomerization of reactive alkanes, with polarizable C−H bonds with adjacent tertiary or quaternary carbon atoms below 370 K. The presence of La^{3+} cations also enhances the zeolite catalyzed hydride transfer rate for isobutane alkylation with 2-butene leading to high catalyst stability. Solid state MAS NMR shows that the strongest positive effects are associated with nonhydroxylated La^{3+} cations accessible to the reacting molecules in supercages of the zeolite. The high activity is the result of a cooperative polarization of C−H bonds of alkanes by La^{3+} cations and the presence of stable and strong Brønsted acid sites.

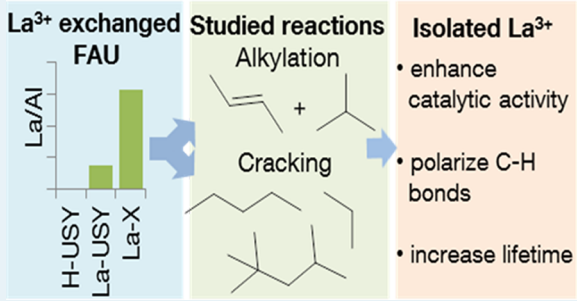

KEYWORDS: *alkylation, cracking, La^{3+} exchange, hydride transfer, C−H bond polarization*

1. INTRODUCTION

Because of the present challenges in adapting the well-proven catalytic chemistry to new feedstocks and decentralized processing (including conversions at or near the source of oil production), novel highly active and stable catalysts have to be developed. The fundamental problem lies in the challenge that usually highly active catalysts for hydrocarbon conversions are always strongly interacting and adsorbing reactants and products alike. We have shown, however, that rare earth exchanged zeolite X has unusual abilities to activate C−H bonds close to ambient temperatures.[1]

Rare earth exchanged zeolites are widely used in refining processes. The rare earth cations stabilize the molecular sieves against dealumination and maintain a higher concentration of acid sites during typical operations as catalysts in fluid catalytic cracking.[2−4] Cation exchanged zeolites polarize and activate CH bonds of alkanes resulting in higher activities and enhanced hydride and hydrogen transfer activities.[1,5]

The presence of La^{3+} has a marked impact upon zeolite catalytic properties. The catalyst stability in isobutane/2-butene alkylation, for example, is significantly improved, partly because La^{3+} increases the concentration of strong Brønsted acid sites (SBAS)[5] by preventing hydrolysis and dealumination during the pretreatment cycles of the catalyst. Strong Lewis acid sites, which are present in higher concentrations in La^{3+}-free catalysts, promote the formation of highly unsaturated carbonaceous deposits causing catalyst deactivation during alkylation reactions.[6−8]

In order to better specify the specific role of the La^{3+} cations, we turn to the mechanism of liquid phase alkylation of isobutane with 2-butene. Scheme 1 summarizes the mechanism

Scheme 1. Mechanism of Isobutane/2-Butene Alkylation Involving the Protonation of 2-Butene, Alkene Addition, Isomerization, and Hydride Transfer[a]

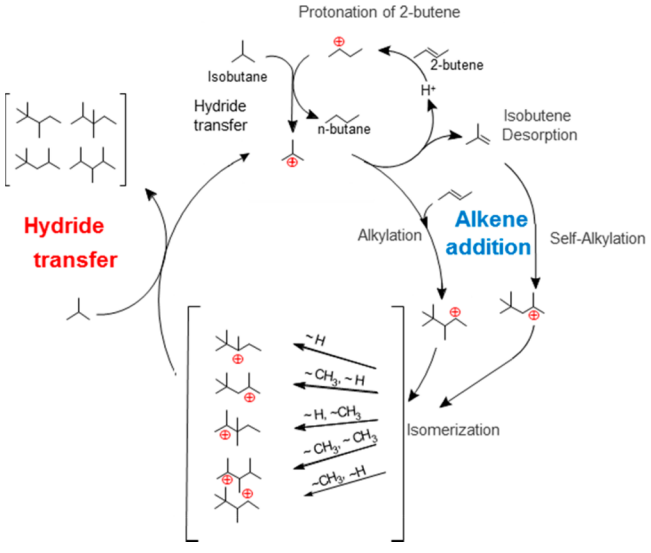

[a]Note that self-alkylation with in-situ formed isobutene is an additional reaction pathway.

of isobutane/2-butene alkylation. The cycle is composed of the alkene addition to the *tert*-butyl carbenium ion (or the

Received: February 14, 2014
Revised: April 14, 2014
Published: April 15, 2014

   dx.doi.org/10.1021/cs500200k | ACS Catal. 2014, 4, 1743−1752

corresponding alkoxide on the solid acid surfaces) formed via hydride transfer from isobutane to the *sec*-butyl carbenium ion generated by 2-butene protonation and the hydride transfer from isobutane to the alkylation products. The 2,2,3-trimethylpentyl carbenium ion is the primary alkylation product, which rapidly isomerizes to other TMPs via successive hydride and methyl shifts. In addition, self-alkylation of surface *tert*-butoxide with in situ formed isobutene is a second reaction pathway which results in the formation of a 2,4,4-trimethylpentyl carbenium ion.[9] The cycle closes by hydride transfer from isobutane to the trimethylpentyl carbenium ion forming trimethylpentane (TMP) and a *t*-butyl carbenium ion. The main reaction pathway for the formation of *n*-butane involves hydride transfer from isobutane to a *sec*-butoxy surface-active species, formed by the adsorption of 2-butene on a free Brønsted acid site (Scheme 1). A high concentration of catalytically active Brønsted acid sites favors a high ratio of carbenium ions to 2-butene and reduces the probability of addition of several 2-butene molecules. La^{3+} drastically enhances hydride transfer and reduces the residence time of the reactive intermediates minimizing further the chance of adding more than one 2-butene molecule.

We explore in this article the unique impacts of the concentration and location of La^{3+} cations on the catalytic activity of USY and X type zeolites. To generate a broad relationship between the acid−base and the remarkable catalytic properties for low temperature acid catalysis, the alkylation of isobutane with 2-butene, propane, and *n*-pentane cracking, and 2,2,4-TMP isomerization and cracking are compared.

2. EXPERIMENTAL SECTION

2.1. Materials. La exchanged zeolite X (La-X) was prepared from Na-X (Si/Al = 1.2), provided by Chemische Werke, Bad Köstritz. The parent material was ion exchanged twice with 0.2 M $La(NO_3)_3$ solution at 353 K for 2 h with a liquid-to-solid ratio of 11 mL/g. The material was washed subsequently with bidistilled water and dried at room temperature. Afterward, the sample was calcined in flowing synthetic air at 723 K for 1 h. After rehydration, three additional ion exchange steps were carried out (for details of preparation see refs 2 and 9). H-USY (Si/Al = 3.1, Na = 0.18 mmol g^{-1}) from Grace Davison was used for the synthesis of La-USY. First the sample was ion exchanged in 0.5 M $La(NO_3)_3$ with a liquid-to-solid ratio of 7 mL/g at 373 K for 4 h. After washing and drying at 373 K for 6 h, the resulting material was calcined in synthetic air at 823 K for 4 h. In order to remove the remaining Na^+ cations from the zeolite, the material was exchanged with 5 M NH_4NO_3 solution over 4 h at 373 K. After filtration, the same drying and calcination procedure described above was applied. The catalysts compared here are equivalent to La-USY I and La-X II described in ref 10.

2.2. Physicochemical Characterization. The concentrations of Al, Si, and Na were determined by atomic absorption spectroscopy (AAS) using a Solaar M5 absorption spectrometer (ThermoFisher). The La^{3+} concentration was determined by ICP-OES (SpectroFlame FTMOA81A from Spectro Analytical Instruments). The pore size distributions and BET surface areas were measured by N_2 physisorption using a PMI automated BET sorptometer.

The nature and concentration of acid sites was analyzed by infrared spectroscopy of adsorbed pyridine. The samples were pressed into self-supporting wafers and activated in vacuum (0.1 mPa) at 723 K for 1 h with a heating rate of 10 K min^{-1}. Pyridine was then adsorbed at 423 K at a pressure of 10 Pa until no further changes were observed. The system was outgassed for 1 h at 423 K to remove all of the physisorbed pyridine. The concentration of strong acid sites was probed by increasing the temperature to 723 K for 0.5 h. Acid sites that retained pyridine were classified as strong Brønsted acid sites (SBAS) and strong Lewis acid sites (SLAS). The Brønsted and Lewis acid sites were discriminated based on the integrals of the IR bands at 1540 and 1450 cm^{-1}, respectively.[11] For quantification, the molar extinction coefficient of 0.73 for Brønsted acid sites and 0.96 for Lewis acid sites was used. These extinction coefficients were determined for a standard material using a combination of thermogravimetric and infrared measurements of the stability of adsorbed pyridine.

For ^{27}Al MAS NMR measurements, the samples were fully rehydrated. The samples were packed into a 4 mm ZrO_2 rotor and measured on a Bruker AV500 spectrometer (B_0 = 11.7 T) with a spinning rate of 12 kHz. For the ^{27}Al MAS NMR single pulse experiment, 2400 scans were recorded using a recycle time of 0.25 s. The excitation pulse had a length of 0.46 μs, which corresponds to a $\pi/12$-pulse. The chemical shifts are reported relative to an external standard of solid $Al(NO_3)_3$ (δ = −0.5427 ppm). The deconvolution of the corresponding MAS NMR spectra was done by using Grams Software (version 7.02). The quantitative analysis was performed as described in ref 10.

For ^{29}Si MAS NMR spectra, 10000 scans were recorded at a resonance frequency of 99.3308 MHz and a recycle time of 5 s. The spectra were referenced against $Si(SiMe_3)_4$ at −9.843 ppm. Deconvolution of the spectra (Grams version 7.02; using 5 Gaussian functions) was done in order to quantify the relative content of Si with 0, 1, 2, 3, and 4 Al neighbors.[1]

^{139}La NMR of La-X and La-USY were measured in static mode. The resonance frequency was 70.6 MHz, and 1×10^6 scans were taken. A Hahn echo pulse sequence was applied.[12] The p_1 and p_2 pulse lengths were 0.8 s, and the pulse delay was 10 μs. The recycle rate was 200 ms. The peak positions were referenced against $LaCl_3$ (0 ppm). All samples for ^{139}La NMR spectroscopic measurements were prepared and measured by the published procedures.[13,14]

Powder X-ray diffraction (XRD) patterns were measured on a Philips X'pert diffractometer equipped with an X'celerator module using CuKα radiation. Diffractograms were obtained from 5 to 75° 2Θ with a step size of 0.033°. The unit cell dimension was calculated from the X-ray diffraction pattern of the zeolite mixed with 5% silicon reference.[15]

2.3. Catalytic Reactions. The purities of the reactants and diluents used were as follows: isobutane 99.95%, 2-butene 99.5%, *n*-pentane 99.7%, propane 99.9%, He 99.999%, and synthetic air 99.999%.

2.3.1. Isobutane/2-Butene Alkylation Reaction. The alkylation of isobutane/2-butene was performed in a 50 mL CSTR (Autoclave Engineers; Mahoney-Robinson spinning basket reactor (1600 rpm)) at 348 K and 2.5 MPa.[9,16] The olefin space velocity (OSV) was 0.2 ($g_{butene}\ g^{-1}{}_{catalyst} h^{-1}$).[9] The isobutane/2-butene ratio was 10/1. The catalysts were activated in H_2 (20 mL) at 393 K for 4 h and at 453 K for 14 h with a heating ramp of 2 K min^{-1}. The product distribution was analyzed using a 50 m HP-1 column (ID = 0.32 mm) in a HP6890 chromatograph equipped with an FID detector.

2.3.2. Protolytic Cracking of Alkanes. The cracking of propane and *n*-pentane was performed in a plug flow reactor

dx.doi.org/10.1021/cs500200k | ACS Catal. 2014, 4, 1743−1752

(length = 350 mm; inner diameter = 6 mm, quartz) at atmospheric pressure. The catalysts (particle size: 250−325 μm) were activated in situ at 803 K with a temperature ramp of 2 K min^{-1} for 2 h in synthetic air (20 mL min^{-1}). Before introducing the reactant (3.0 vol % for propane and 2.0 vol % for *n*-pentane, in He), the reactor was flushed for 30 min with pure He. The catalytic reaction was performed between 753 and 793 K. The conversion was kept below 1.5% in order to avoid contributions from products of the bimolecular or secondary reaction pathways, the absence of which was confirmed by the equimolar ratio of ethylene to methane. For *n*-pentane cracking, a contribution of secondary cracking of the dehydrogenation product pentene was observed despite the low conversions. Reactants and products were separated and analyzed by online chromatographic measurements (HP 5890, capillary column: HP-Al_2O_3/KCl, 50 m × 0.32 mm × 8.0 μm) with an FID detector. The apparent activation energies for the protolytic cracking of propane and *n*-pentane were determined from the slopes of the Arrhenius plots in a temperature range of 753−783 K. The corresponding activation entropies were obtained using transition state theory.

2.3.3. Isomerization and Cracking of 2,2,4-TMP. The conversion of 2,2,4-TMP was studied in the same reactor as that used for the cracking of propane and *n*-pentane. The catalysts (particle size: 150−250 μm) were first activated in situ at 393 K for 4 h and at 453 K for 12 h in H_2 (30 mL min^{-1}). Catalyst stability studies were performed at 368 K using 5.0 mol % of 2,2,4-TMP. Kinetics were measured in the range of 348−368 K. Then, 5.0 mol % of 2,2,4-TMP was introduced into He (9.7 mL min^{-1}) using a saturator with three consecutive saturation flasks kept at the desired saturation temperature; the first two were filled with 2,2,4-TMP, while the last was empty. The reactant and products were analyzed with online GC (HP 5890; capillary column, HP-1 column; 50 m × 0.32 mm × 0.52 μm).

3. RESULTS

3.1. Chemical Composition and Physicochemical Properties. The chemical composition and the physicochemical properties of the studied materials are compiled in Table 1. The absolute concentration of La^{3+} cations and the concentration relative to Al^{3+} was much higher in La-X (0.315) than in La-USY (0.074). The ratio of La^{3+} exchanged per Al containing tetrahedron of the zeolite should be 1/3, when assuming a nonhydroxylated La^{3+} cation.[10] This value was only approached with zeolite X. The micropore volumes, as well as the unit cell sizes and the intensity of the diffractogram, show that the preparation procedures did not affect the crystal structures. In both La^{3+} exchanged zeolites, the Na^+ content was low, 1.5 and 0.2%, respectively, of the maximum exchange capacity. These remaining Na^+ cations located in the hexagonal prism or six-membered ring openings of the sodalite cages hardly influenced the reactions because both locations are inaccessible to the hydrocarbons.[10,17]

USY had a much higher concentration of total and strong Brønsted acid sites (H-USY = 0.513 $mmol_{SBAS}/g_{catalyst}$ and La-USY = 0.557 $mmol_{SBAS}/g_{catalyst}$) compared to La-X (0.062 $mmol_{SBAS}/g_{catalyst}$). The low concentration of Brønsted acid sites in the LaX is caused by the high ratio of La/Al leaving only a relatively small concentration of Al tetrahedra that were able to form bridged hydroxy groups. The concentration of strong Lewis acid sites was much higher for H-USY and La-USY than for La-X.

The local environments of Al in H-USY, La-USY, and La-X were investigated by ^{27}Al MAS NMR and ^{29}Si MAS NMR and shown in Figure 1. Peaks for tetrahedrally (60−40 ppm) as well as octahedrally coordinated Al (ca. 0 ppm) were found for all samples. The concentrations of octahedrally coordinated Al in H- and La-USY (24.8 and 18.8%, respectively) were higher than those in La-X (7.0%). The Al corresponding to the peak at 58 ppm was tetrahedrally coordinated and the charge on the tetrahedron compensated by H^+ and Na^+. The strong distortion of the peak at 45 ppm in La-X is attributed to the presence of La^{3+} cations compensating the charge of three Al−O tetrahedra.[9] With La-USY, only a shoulder was observed at 45 ppm because the much lower concentration of Al in the lattice makes the presence of three proximate Al−O tetrahedra that can be compensated by a single La^{3+}improbable.

The corresponding ^{29}Si MAS NMR spectra and the number of Al neighbors are exhibited in Figure 1 and compiled in Table 2, respectively. In the ^{29}Si MAS NMR spectra, the peak

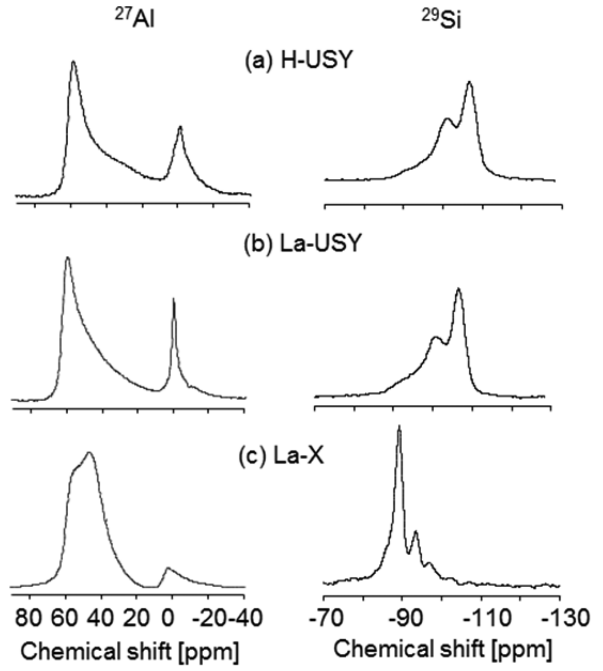

Figure 1. ^{27}Al (left) and ^{29}Si (right) MAS NMR sprectra of H-USY (a), La-USY (b), and La-X (c) partly reproduced from ref 10. Copyright 2011 American Chemical Society.

Table 1. Physicochemical Properties and Acid Site Distributions of H-USY, La-USY, and La-X

	H-USY	La-USY	La-X
Si/Al	3.1	4.0	1.2
Al/unit cell in framework	28.0	27.2	79.4
unit cell size [nm]	2.45	2.45	2.49
Na/Al	0.060	0.015	0.002
La/Al	0	0.074	0.315
micropore volume [cm^3/g]	0.28	0.26	0.26
BAS[a] [mmol/g]	0.10	0.92	0.37
LAS[b] [mmol/g]	0.44	0.42	0.55
SBAS [mmol/g]	0.51	0.56	0.06
SLAS [mmol/g]	0.30	0.28	0.06

[a]BAS = Brønsted acid sites. [b]LAS = Lewis acid sites.

dx.doi.org/10.1021/cs500200k | ACS Catal. 2014, 4, 1743−1752

Table 2. Tetrahedrally (tetr.) and Octahedrally (oct.) Coordinated Al Determined by ^{27}Al MAS NMR as Well as Al Linked to Si Determined by Deconvolution of ^{29}Si MAS NMR

catalyst	tetr. Al [%]	oct. Al [%]	Si(0Al) [%]	Si(1Al) [%]	Si(2Al) [%]	Si(3Al) [%]	Si(4Al) [%]
H-USY	75	25	39	57	4		
La-USY	81	19	34	55	11		
La-X	93	7	4	9	9	11	67

positions are shifted upfield by about 4 ppm by the presence of La^{3+} cations. This is attributed to wider Al−O−Al or Al−O−Si bond angles in the six ring windows of the sodalite cages in agreement with observations by Klein et al. and Gaare et al.[17,18] In line with the differences in the stabilization of the La^{3+} cations through multiple exchange sites, most Si atoms of H-USY and La-USY have 0 or 1 Al neighbor, while in La-X most Si tetrahedra have 3 or 4 neighboring Al−O tetrahedra (Table 2).

The locations of La^{3+} cations were investigated by ^{139}La NMR. The spectra are shown in Figure 2. The charge

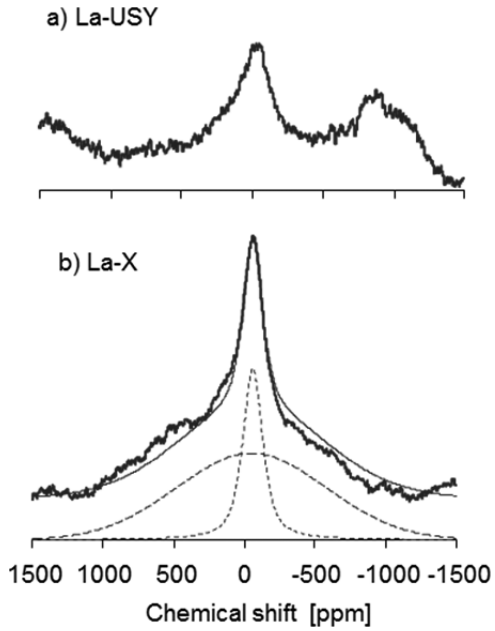

Figure 2. ^{139}La NMR of La-USY (a) and La-X (b): experiment (—) and theoretical fit (- - -).

distribution around (the inaccessible) La^{3+} cations in the center of 6-membered O rings inside the sodalite cages caused a large quadrupolar coupling.[10] Consequently, a very broad line with a width of 190 ± 10 kHz was observed. La^{3+} cations in supercages are more mobile and create, in particular when they are fully hydrated, a smaller electric field gradient and a smaller quadrupolar coupling. In the spectrum of La-X, a sharp peak at −67 ppm with a line-width of 11.7 kHz was observed (Figure 2b), together with a second broad peak having the same chemical shift but a line width of 87.6 kHz. Following Hunger et al.,[19] we attribute, thus, the narrow line to La^{3+} in the FAU supercages, and the broad line is attributed to La^{3+} cations in the sodalite cages. The width of the broad line was approximately half of the value published previously, suggesting an increased structural flexibility of the present materials. Simulations of the spectrum of La-X (Figure 2b) showed that approximately 25% of the incorporated La^{3+} were located in the supercages.

The signal of La^{3+} cations in La-USY had lower intensity consistent with lower La^{3+} content. Therefore, only one relatively sharp line was observed at −32 ppm with a width of 22.0 kHz (Figure 2a). The peak was assigned to $[La(OH)_2]^+$ and $[La(OH)]^{2+}$. The occupancy of supercages by La^{3+} was low.

3.2. Catalyzed Reactions. *3.2.1. Alkylation of Isobutane/2-Butene.* The alkylation of isobutane with 2-butene can only be studied in a meaningful way, if the concentration of 2-butene is kept so low that oligomerization is largely avoided. This is because the oligomerization of 2-butene, responsible for a low product quality and early catalyst deactivation, has a substantially higher forward rate than hydride transfer and other reactions associated with alkylation.[20,21] Table 3 compiles the analysis of individual compounds and compound groups produced after 20 h time on stream (TOS). The products were C_5−C_7 hydrocarbons, various C_8 isomers, and small amounts of larger alkanes (C_{9+}). The C_5−C_7 products were formed from cracking via β-scissions, whereas the C_{9+} products originated from multiple alkylation on strong Brønsted acid sites and oligomerization on the weaker Brønsted acid sites.

The C_8 fraction, in particular trimethylpentanes, which are important for the alkylate quality, constituted 69−79 wt % of the total C_{5+} yield over the lifetime of each catalyst (Table 3). Within the C_8 fraction, low amounts of dimethylhexanes and even smaller amounts of methylheptanes were formed by slow isomerization of TMP transiently generated via a protonated cyclopropane intermediate. *n*-Butane was produced in substantial amounts over the entire TOS of 20 h (Table 3). As *n*-butane cannot be formed directly by β-scission of a carbenium ion, the main possible reaction route for its formation involves hydride transfer from isobutane to a *sec*-butoxy surface species formed in the initiating reaction step by adsorption of 2-butene on a strong Brønsted acid site (Scheme 1). Since the primary products of isobutane/2-butene alkylation were 2,2,3-TMP and 2,2,4-TMP for self-alkylation, the C_8 product distribution was used to evaluate the relative rates of hydride transfer and isomerization.

Table 3. Product Distribution Following the H-USY, La-USY, and La-X Catalyzed Alkylation of Isobutane/2-Butene[a]

catalyst	lifetime at full conversion [h]	C_{5-7} [g $g_{cat.}^{-1}$] (wt %)	C_8 [g $g_{cat.}^{-1}$] (wt %)	C_{9+} [g $g_{cat.}^{-1}$] (wt %)	*n*-butane [g $g_{cat.}^{-1}$]
H-USY	5	0.26 (11.1)	1.68 (71.5)	0.41 (17.4)	0.05
La-USY	12	0.98 (17.8)	3.85 (68.9)	0.68 (12.3)	0.22
La-X	16	0.92 (10.9)	6.68 (78.9)	0.87 (10.2)	0.29

[a]Reaction conditions: temperature = 348 K, isobutane/2-butene = 10, olefin space velocity (OSV) = 0.2 h^{-1}, and stirring speed = 1600 rpm.

dx.doi.org/10.1021/cs500200k | ACS Catal. 2014, 4, 1743−1752

The catalyst lifetime, defined as the time to 99.5% 2-butene conversion, is the most important parameter to evaluate the efficacy of the catalysts.[5,22] The lifetime of such catalysts has been correlated for a given set of operation conditions to the rate constant of hydride transfer between isobutane and the carbenium ions, as well as to the concentration of Brønsted acid sites determining the concentration of carbenium ions. In the present case, the incorporation of La^{3+} into USY extended the catalyst lifetime from 5 to 12 h (Table 3).

For La-X, the catalyst lifetime was even further increased to more than 16 h, although the catalyst had a significantly lower concentration of strong Brønsted acid sites (0.06 mmol SBAS/$g_{catalyst}$) than the other two (0.51, 0.56 mmol SBAS/$g_{catalyst}$).

The presence of La^{3+} reduced the relative rate of multiple alkylation (fraction of C_{9+} in the products). The selectivity to C_{9+} decreased from H-USY through La-USY to La-X by more than 40% despite the much increasing overall amounts of product hydrocarbons (Table 3). The relative rate to C_{9+} was constant for H-USY over the time the catalyst was active (Figure 3a), while it was negligible for the La^{3+} containing

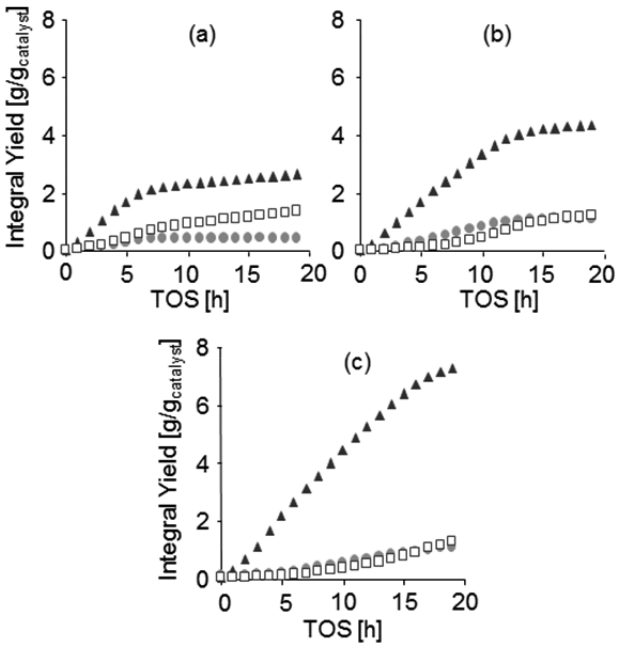

Figure 3. Total product yields of C_5−C_7 (●), C_8 (▲), and C_{9}^{+} (□) in the presence of H-USY (a), La-USY (b), and La-X (c). Activation procedure: in situ in H_2, 4 h at 393 K and 14 h at 453 K, and heating ramp = 2 K min^{-1}. Reaction conditions: reaction temperature = 348 K, isobutane/2-butene = 10, OSV = 0.2 $g_{butene}g_{catalyst}^{-1}h^{-1}$, stirring speed = 1600 rpm.

catalysts for the first 3−5 h (Figure 3b,c) and increased only as the catalyst approached the end of its lifetime. This shows that La^{3+} initially decreased the lifetime of the carbenium ions, thus decreasing the yield of heavier products.

The effect of La^{3+} incorporation on catalyst selectivity to TMP, dimethyl hexane (DMH), and methyl heptanes (MHp) is compiled in Table 4. The selectivity in the C_8 fraction is shown in Figure 4 as a function of time on stream. The selectivity for each product was integrated until the start of the deactivation, i.e., when the conversion of 2-butene dropped below 99.5%.

Table 4 shows that TMPs were the most abundant products (90 wt % of the total C_8 fraction). The high 2,2,4-TMP

Table 4. Detailed Product Distribution within the Octane (C_8) Fraction in Solid Acid Catalyzed Alkylation of Isobutane/2-Butene[a]

selectivity	H-USY [%]	La-USY [%]	La-X [%]
2,4-DMH	2.49	4.52	3.35
2,3-DMH	5.35	4.95	4.37
2-MHp	0.01	0.23	0.16
4-MHp (3,4-DMH)	0.92	0.73	0.71
3,4-DMH (4-MHp)	0.71	0.86	0.85
3-MHp	0.10	0.26	0.15
2,5-DMH/2,2,3-TMP	5.94	11.61	10.10
2,2,4-TMP	20.80	35.32	26.10
2,3,3-TMP	33.62	24.20	32.73
2,3,4-TMP	29.37	16.97	21.25
∑ TMP	89.73	88.1	90.18
∑ DMH	8.55	10.33	8.57
∑ MHp	1.03	1.22	1.02

[a]Reaction conditions: temperature = 348 K, isobutane/2-butene = 10, OSV = 0.2 g_{butene} $g_{catalyst}^{-1}h^{-1}$, and stirring speed = 1600 rpm. DMHs, dimethylhexanes; MHps, methylheptanes; TMPs, trimethylpentanes

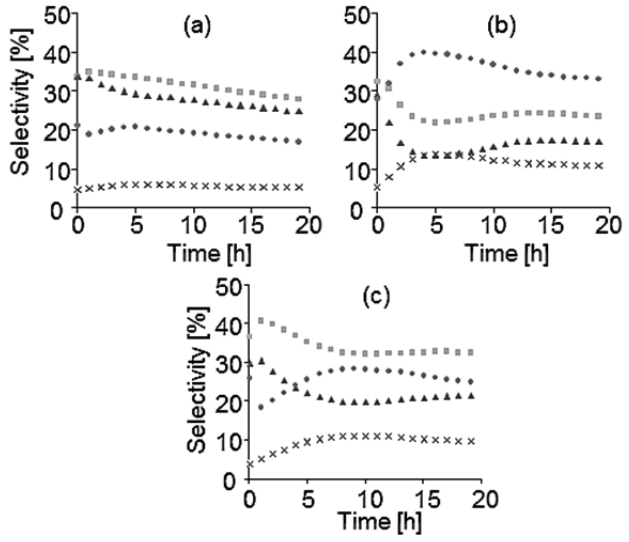

Figure 4. Product selectivity of 2,5-DMH/2,2,3-TMP (×), 2,2,4-TMP (●), 2,3,3-TMP (■), and 2,3,4-TMP (▲) over H-USY (a), La-USY (b), and La-X (c). Reaction conditions: T = 348 K, isobutane/2-butene = 10, OSV = 0.2 $g_{butene}g_{catalyst}^{-1}h^{-1}$, and stirring speed = 1600 rpm.

selectivity suggests that self-alkylation, i.e., the intermediate generation of isobutene via hydride transfer from *n*-butyl carbenium ions, significantly contributed to isobutane/2-butene alkylation.[9] The presence of La^{3+} in USY increased the selectivity for 2,2,4- and 2,2,3-TMP, indicating a faster hydride transfer rate relative to alkylation. In contrast to La-USY, increasing La^{3+} concentration in La-X lowered the selectivity for 2,2,4-TMP and significantly increased the selectivity for 2,3,4-TMP and 2,3,3-TMP isomers under the same reaction conditions (Figure 4).

The product yields of C_8 olefins and *n*-butane from catalytic iso-butane alkylation (Figure 5) showed that self-alkylation in the presence of H-USY was slow relative to the formation of unsaturated octane isomers. The absolute rates and the relative importance of self-alkylation increased drastically in the presence of La^{3+}. Note that C_8 olefins began to be formed

dx.doi.org/10.1021/cs500200k | ACS Catal. 2014, 4, 1743−1752

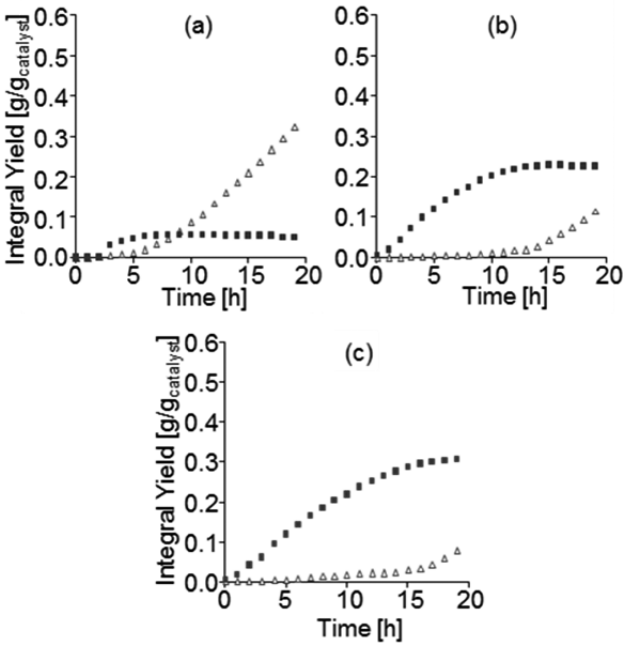

Figure 5. Product yield of unsaturated C_8 (△) and *n*-butane (■) as a function of time on stream (TOS) over H-USY (a), La-USY (b), and La-X (c). Reaction conditions: T = 348 K, isobutane/2-butene = 10, OSV = 0.2 h^{-1}, and stirring speed = 1600 rpm.

once the level of 2-butene conversion had dropped below 99.5%.

3.2.2. Protolytic Cracking of Alkanes. The rate constants, the activation energies and the entropies of protolytic cracking and dehydrogenation of propane and *n*-pentane at 773 K over modified and unmodified zeolites are compiled in Tables 5 and 6. The overall rate constant for cracking (i.e., the sum of all rate constants for the individual pathways) increased by a factor of 2 and that for dehydrogenation by a factor of 3 as the concentration of accessible La^{3+} sites in the catalysts increased. The activation energy for propane cracking (156 kJ/mol) on the parent ultrastable zeolite Y was comparable to that (166 kJ/mol) reported by Xu et al.[24] for H-USY (Si/Al = 2.5) in a temperature range of 675−875 K and a propane partial pressure of 10 kPa. The activation energies were lower by 22−46 kJ/mol and entropies by 39−72 J/(mol K) for propane dehydrogenation than for cracking on all catalysts. For H-USY and La-USY (Ea_{app} = 131 kJ/mol and ΔS_{app} = −155 J/(mol K), however, higher activation energy and entropy were obtained for the dehydrogenation of propane compared to that for La-X (Ea_{app} = 104 kJ/mol and ΔS_{app} = −185 J/mol K). La-X had a higher fraction than La-USY of accessible, nonhydroxylated La^{3+} cations at SII positions in supercages (0.99 mmol/g and 0.16 mmol/g, respectively) that are able to activate secondary and tertiary C−H bonds.[10] The facile dehydrogenation might be related to the unique capability of La^{3+} in La-X to stabilize a hydride anion and support the ionic elimination of H_2.

The corresponding measured apparent first order rate constants (k_{app}) at 773 K, activation energies, and entropies for *n*-pentane conversion over the same samples are summarized in Table 6 and are shown in Figure 6. The measured rate constants for monomolecular cracking of *n*-pentane were >10-fold larger compared to those of propane. In *n*-pentane, two equivalent central C−C bonds exist. Depending on the carbon being attacked by the proton, cracking at this bond can proceed via two different pathways leading to C_2 and $C_3^=$ or to C_3 and $C_2^=$. The formation of C_2 and $C_3^=$ is 4−11 kJ/mol favored over the formation of C_3 and $C_2^=$. Entropies of activation decrease from the terminal to inner C−C bonds. The more negative activation entropy values for the cleavage of the central bonds reflect the lower configurational entropy of the more symmetric carbonium ion. For all cracking pathways, the measured energies and entropies of activation decreased with increasing La^{3+} content of the zeolite, similar to the trend for the apparent activation energies observed with propane. However, activation entropies remain constant with increasing La^{3+} content in the case of propane.

For both studied molecules, the energy barriers for cracking were lower in the presence of sites involving isolated La^{3+}. For H-USY and La-USY, the activation energies of dehydrogenation of propane were 20 kJ/mol lower than the activation energies for total cracking, whereas in the case of *n*-pentane it was 10 kJ/mol higher. For both molecules, the energy barriers for the dehydrogenation pathway were influenced in the same manner in the presence of La-X resulting in a drop of activation energy and activation entropy when compared to those in H-USY and La-USY.

3.2.3. Catalytic Conversion of 2,2,4-TMP. All catalysts deactivated rapidly at the start of 2,2,4-TMP conversion (Figure 7). Measured rates normalized to the concentration of strong BAS (turnover frequency) on H-USY and La-USY under steady state conditions were similar, while on La-X they were higher up to factor of 6 (Table 7).

The apparent activation energies increased with the loading of La^{3+}. The presence of La^{3+} in La-USY, however, did not significantly enhance the rate constant of 2,2,4-TMP conversion (Figure 8 and Table 7). This is in agreement with the conclusion that only a small concentration of La^{3+} was accessible and most of that was hydroxylated, diminishing its impact.[10,25] Catalytic cracking dominated forming iso-butane,

Table 5. Measured Rate Constants (k), Activation Energies (Ea_{meas}), and Entropies (ΔS_{meas}) for Monomolecular Propane Cracking (C) and Dehydrogenation (D) over H-USY, La-USY, and La-X[a]

catalyst	H-USY	La-USY	La-X	H-USY	La-USY	La-X	H-USY	La-USY	La-X
pathway	k[b] [10^{-3} mol/(mol$_{SBAS}$·Xs·bar)]			Ea_{app}[c] [kJ/mol]	Ea_{app}[d] [kJ/mol]	Ea_{app}[e] [kJ/mol]	ΔS_{app}[f] [J/(mol K)]	ΔS_{app}[g] [J/(mol K)]	ΔS_{app}[h] [J/(mol K)]
$C_1 + C_2^=$	0.70	0.55	1.48	156	154	150	−111	−116	−113
$C_3^= + H_2$	0.20	0.15	0.61	131	132	104	−155	−155	−185
C/D ratio	3.5	3.7	2.5						

[a]All catalysts were activated in situ in synthetic air (20 mL min^{-1}) for 2 h at 803 K (2 K min^{-1}). Reactions were performed in a temperature range of 753−783 K with 10 K intervals at propane partial pressure = 0.03 bar. Entropies were derived according to transition state theory.[23] [b]Rate constants were determined at 773 K. [c]±2 kJ/mol. [d]±6 kJ/mol. [e]±7 kJ/mol. [f]±4 J/ (mol K). [g]±8 J/(mol K) [h]±14 J/(mol K).

dx.doi.org/10.1021/cs500200k | ACS Catal. 2014, 4, 1743−1752

Table 6. Measured Rate Constants, Activation Energies (Ea_{meas}), and Entropies (ΔS_{meas}) for Monomolecular *n*-Pentane Cracking in Terms of Different Pathways over H-USY, La-USY, and La-X[a]

catalyst	H-USY	La-USY	La-X	H-USY	La-USY	La-X	H-USY	La-USY	La-X
pathway	k[b] [10^{-3} mol/(mol$_{SBAS}$·s·bar)]			Ea_{app}[c] [kJ/mol]	Ea_{app}[d] [kJ/mol]	Ea_{app}[e] [kJ/mol]	ΔS_{app}[f] [J/ (mol K)]	ΔS_{app}[g] [J/(mol K)]	ΔS_{app}[h] [J/(mol K)]
$C_1 + C_4^=$	4.4	2.0	14.9	153	147	136	−103	−113	−122
$C_2 + C_3^=$	5.3	3.7	20.0	139	134	128	−120	−128	−132
$C_3 + C_2^=$	2.5	9.4	8.5	150	142	132	−112	−125	−132
overall cracking	12.2	15.1	43.4	147	140	131	−103	−114	−120
$C_5^= + H_2$	10.1	12.6	15.3	158	152	109	−105	−115	−169
C/D ratio	1.2	1.2	2.8						

[a]All catalysts were activated in synthetic air (20 mL min^{-1}) for 2 h at 803 K (2 K min^{-1}). Reactions were performed in a temperature range of 753−783 K with 10 K intervals, pentane partial pressure =0.02 bar. Entropies were derived according to transition state theory.[23] [b]Rate constants were determined at 773 K. [c]±2 kJ/mol. [d]±3.5 kJ/mol. [e]±3 kJ/mol. [f]±5 J/ (mol K). [g]±3 J/ (mol K) [h]±3 J/ (mol K).

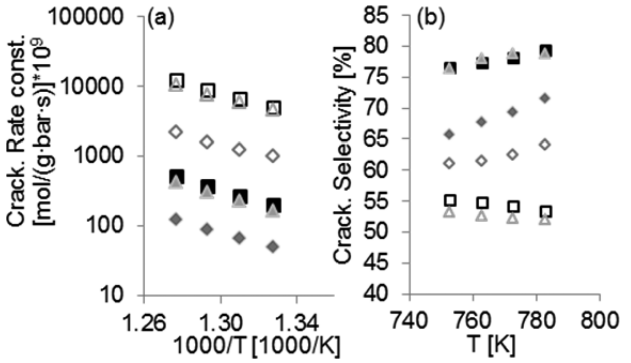

Figure 6. Rate constants (a) and selectivities (b) of propane (closed symbols) and *n*-pentane (open symbols) protolytic cracking with H-USY (■), La-USY (▲), and La-X (♦) catalysts. Activation: synthetic air (20 mL min^{-1}) and 2 h at 803 K (2 K min^{-1}). Reaction: temperature range 753−783 K and propane (*n*-pentane) partial pressure of 0.03 (0.02) bar.

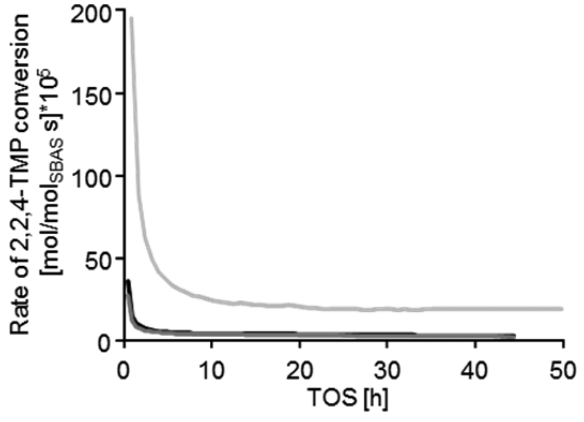

Figure 7. Rate of 2,2,4-TMP conversion with increasing time on stream over H-USY (black), La-USY (gray), and La-X (light gray) catalysts. Activation was in H_2 (30 mL min^{-1}) for 4 h at 393 K and 12 h at 453 K. Reaction: 368 K and 5 mol % 2,2,4-TMP in He (9.7 mL min^{-1}).

and the selectivity to isomerization never exceeded 30%. The selectivity for cracking increased moderately with La^{3+} loading. At 348 K, for example, 73% of the converted 2,2,4-TMP was cracked on La-USY, while on La-X 87% was cracked.

After 5 and 45 h on stream, a lower concentration of coke was deposited on La-X (8.8 wt %) than on H-USY or La-USY (10.5 wt %). Thermogravimetric analysis indicated that under reaction conditions H-USY Brønsted acid sites were covered with 2,2,4-TMP in line with the observed reaction order of zero. The true activation energies under these conditions increased for cracking and isomerization of 2,2,4-TMP with the loading of La^{3+} (Table 7). The estimated reaction enthalpy for catalytic cracking of 2,2,4-TMP was 77 ± 0.1 kJ/mol, while the calculated reaction entropy was 168 ± 0.3 J/(mol K).[26] The maximum possible conversion was, therefore, 2.4% at 318 K and 15.9% at 368 K, based on the calculated equilibrium constants. A slightly higher selectivity to isobutane was found for La-X compared to the other two catalysts.

4. DISCUSSION

La^{3+} stabilizes the faujasite lattice.[9] The influence of La^{3+} on the catalytic properties of faujasite has been intensively discussed without consensus. This reflects that the acid−based properties of the discussed zeolites are complex and that the zeolites contain a range of acid sites. This somewhat limits the present conclusions to structure−activity correlations derived from the physicochemical characterization presented here and in a preceding paper.[10] We used H-USY, La-USY, and La-X because all three have shown stable catalytic performance for alkylation of isobutane with 2-butene, as well as for cracking of propane and 2,2,4-trimethylpentane. All three reactions are catalyzed by Brønsted acid sites but depend to different extents on the hydride transfer and allow in this way a separation of the effect of the intrinsic properties of Brønsted acid sites from indirect influences imposed by the presence of La^{3+} cations.

4.1. Identification of the Nature and Location of La^{3+}.

We first analyze and summarize the location and speciation of the La^{3+} and their potential impact on the acid−base properties of the catalysts. Only for USY is a direct comparison between the presence and absence of La^{3+} possible, as the purely acidic form of zeolite X is thermally unstable. However, a comparison between La-USY and La-X allows evaluating the role of La^{3+}coordination. ^{29}Si and ^{27}Al MAS NMR show that La^{3+} exchange stabilizes pairs of next nearest neighbor Al in the lattice (4% Si(2Al) in H-USY and 11% in La-USY), while the concentrations of isolated Al−O tetrahedra changed inversely. However, the increase of Si−O tetrahedra without Al neighbors suggests that the difference between the stability of nearest neighbor Al pairs and isolated Al must be small. In the case of a marked difference in stability, the disappearance of Si(2Al) should have been compensated by an equally large increase in the concentration of Si(1Al) (Table 2).

dx.doi.org/10.1021/cs500200k | ACS Catal. 2014, 4, 1743−1752

Table 7. Apparent Activation Energies and Pre-exponential Factors for Cracking and Isomerization of 2,2,4-TMP Catalyzed by H-USY, La-USY, and La-X Catalysts[a]

catalyst	H-USY	La-USY	La-X
$E_{A\ cracking}$ [kJ/mol]	35	43	62
$E_{A\ isomerization}$ [kJ/mol]	14	25	50
$k_{cracking}$ [b] [10^{-5} mol/(mol$_{SBAS}$·s·bar)]	69.7	65.3	423
$k_{isomerization}$ [b] [10^{-5} mol/(mol$_{SBAS}$·s·bar)]	16.0	17.3	51.5
$A_{cracking}$ [mol/(g$_{catalyst}$·s·bar)]	3.4×10^{-2}	5.0×10^{-1}	1.6×10^{2}
$A_{isomerization}$ [mol/(g$_{catalyst}$·s·bar)]	7.5×10^{-6}	3.2×10^{-4}	0.39
$A_{cracking/SBAS}$ [mol/(mol$_{SBAS}$·s·bar)]	6.6×10^{1}	9.0×10^{2}	2.6×10^{6}
$A_{isomerization/SBAS}$ [mol/(mol$_{SBAS}$·s·bar)]	1.5×10^{-2}	5.8×10^{-1}	6.4×10^{3}

[a] 2,2,4-TMP cracking: the selected materials were activated in H_2 (30 mL min^{-1}) for 4 h at 393 K and 12 h at 453 K. Catalytic reaction: 348 to 368 at 10 K intervals, 5 mol % 2,2,4-TMP in He (9.7 mL min^{-1}). [b] At 368 K.

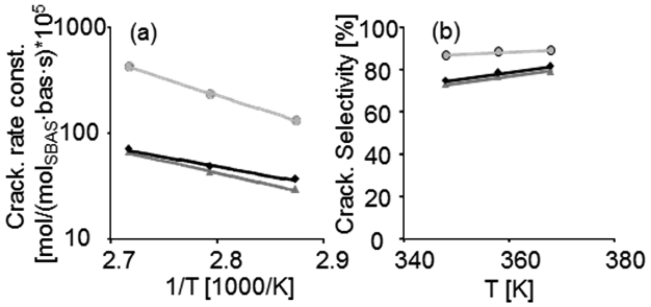

Figure 8. Rate constants normalized by active Brønsted acid sites (a) and cracking selectivity (b) of 2,2,4-TMP conversion on H-USY (♦), La-USY (▲), and La-X (●). Reaction: measurements every 10 K from 348 to 368 K and 5 mol % 2,2,4-TMP in He.

The higher concentration of the extra-framework Al (EFAl) in H-USY compared with La-USY corresponds with the lower concentration of Si(2Al). LaX had a high concentration of Si(4Al) and Si(3Al), and a low concentration of EFAl. The ^{27}Al MAS NMR spectra indicate that La^{3+} caused significant distortion of the zeolite lattice at the ion exchanged sites. Because of the much larger concentration of La^{3+}, the effect was more conspicuous for LaX but clearly discernible also for La-USY. We assigned the line width of 11.7 kHz in the ^{139}La NMR spectra to La^{3+} in the supercage.[14,19] The quantification for La-X (La/Al ratio of 0.315) indicates that a quarter of the La^{3+} are located there. The corresponding peak for La^{3+} cations was drastically weaker for La-USY (Figure 2a) corresponding with the lower concentration of exchanged La^{3+}. The assignments of peaks in refs 14 and 19 indicate that La^{3+} cations in the supercages and sodalite cages of La-USY mainly existed as $La(OH)^{2+}$ or $[La(OH)_2]^+$. The line width for La^{3+} cations in the sodalite cages was 87.6 kHz and significantly narrower than that reported by Hunger et al. (190 ± 10 kHz) and Herreros et al. (150 kHz),[14,19] indicating a higher mobility of these cations in the present case.

The exchange of La^{3+} stabilized the zeolite framework, decreased the maximum concentration of Brønsted acid sites, and increased Lewis acidity. Moreover, as shown in Table 1 for USY materials, the stabilization by La^{3+} of Al in the lattice led to an increase of the strong Brønsted acid sites (bridging hydroxyl groups). This indicates that not only the next nearest neighboring pairs of Al−O tetrahedra (stabilizing preferentially the exchanged La^{3+} cations) but also the isolated bridging OH groups were stabilized by La^{3+}. These acid sites were quantified by adsorbed pyridine, which probes only the accessible sites in the supercages.

The increase of the concentration of Brønsted acid sites and the decrease of the concentration of Lewis acid sites suggests that La^{3+} is located primarily in the sodalite cages in the form of $La(OH)^{2+}$ and that this created strong Brønsted acid sites in the supercages. The mechanism and reason for the stabilization of the Al−O tetrahedra across such a long distance is not understood. The strong Lewis acid sites observed with H-USY and La-USY are caused solely by coordinated unsaturated Al^{3+} cations. La^{3+} cations being much larger than Al^{3+} cations bind pyridine only very weakly, irrespective of the hydroxyl groups attached to them.

The larger concentration of La^{3+} exchanged and especially the higher ratio of La/Al diminished the concentration of Brønsted acid sites in La-X. However, estimating it from the overall concentration of Al and the concentration of octahedral Al in the zeolite, we observed that the relative distribution between the accessible and inaccessible strong Lewis acid sites remained about the same for La-X and La-USY. We have shown in a preceding paper[10] that higher concentrations of La^{3+} lead to repulsion between cations in the sodalite cages, causing about 25% of the La^{3+} cations to be located at SII sites in the supercage. The higher concentration of negative charges of the lattice O stabilizes such positions.

Having discussed the location and nature of the Brønsted and Lewis acid sites and La^{3+} cations, let us turn to the catalytic chemistry of the three Brønsted acid catalyzed reactions. It has been established by previous contributions that accessible La^{3+} cations polarize C−H bonds[10] and generate reactive carbenium ions from alkanes.

4.2. Impact of La^{3+} on Isobutane Alkylation. For alkylation, La^{3+} acts via enhancing hydride transfer. The alkylation of isobutane with 2-butene utilizes these hydride transfer capabilities of La^{3+}. At steady-state, the reaction is controlled by the addition of 2-butene and in situ formed isobutene as well as by the hydride transfer from isobutane to the surface bound alkyl. As the former reaction is easier, alkylation catalysts tend to build over time hydrocarbon deposits that cause deactivation. A higher concentration of Brønsted acid sites suppresses this reaction by reducing the probability that repeated alkylation occurs on a particular carbenium ion. The presence of La^{3+} enhances the selectivity to the second reaction by polarizing the hydride donating isobutane. Especially with La-X, the enhanced cracking rate of branched alkanes protects the catalyst by removing carbonaceous deposits. As a consequence, the productivity of La-X was about four times as high as that of H-USY.

4.3. Catalytic Cracking of Alkanes. *4.3.1. Propane Cracking.* The catalytic activity for the cracking of propane

dx.doi.org/10.1021/cs500200k | ACS Catal. 2014, 4, 1743−1752

increases with the concentration of Brønsted acid sites on all three zeolites investigated. Normalization of the rates to the strong Brønsted acid sites (SBAS) showed, however, an increase in the propane cracking rate by factors of two and more than three for the propane dehydrogenation rate with increasing concentrations of La^{3+} (Tables 1, 5, and 6). The protolytic dehydrogenation of propane is more favored than protolytic cracking by isolated La^{3+} cations close to SBAS, as is the case on La-X, clearly indicating that those sites polarize C−H bonds facilitating at the same time the addition of a proton to the hydride in the activated alkane molecule. This is reflected also in the significantly decreased activation energies for dehydrogenation over La-X (104 kJ/mol) compared to those of the other two catalysts (130 kJ/mol).

The catalyst with the highest activity had the lowest concentration of extra-lattice Al so the polarization of the C−H bond induced by accessible La^{3+} was much stronger than that induced by Al^{3+}. This corroborates that the concentration of octahedrally coordinated Lewis acidic extra-framework Al sites did not influence the rate of cracking.[26] In comparison, the polarization of La^{3+} of the C−C bond was less marked, as evidenced from the slight decrease in activation energies and entropies on La-X compared to those in USY catalysts. Therefore, kinetic differences between cracking and dehydrogenation mainly reflect entropic effects of the transition state confinement. As the measured activation entropies were lower on all catalysts by 39−72 J/(mol K) for the protolytic dehydrogenation of propane than for cracking, a more tightly bound transition state is indicated in the presence of La^{3+}.

4.3.2. n-Pentane Cracking. The cracking of *n*-pentane can proceed by multiple pathways. Cleavage of the terminal bond leading to C_1 and $C_4^=$ is energetically more demanding than the cleavage of internal C−C bonds. Depending on the C atom protonated, the internal route results either in C_2 and $C_3^=$ or in C_3 and $C_2^=$. The pathway resulting in C_2 and $C_3^=$ is energetically favored by 11 kJ/mol over the alternative pathway on H-USY. If the transition state of cracking was early resembling the reactants, an energetic difference between those two alternative pathways could not be explained. Therefore, we conclude that the transition state is late and resembles the products. However, the differences in the activation energies are decreased with increasing content of accessible La^{3+} sites in the zeolite structure reflecting a better stabilization of the activated transition state species. The higher activation entropy for cracking at the terminal C−C bond shows a higher degree of rotational and vibrational freedom of this transition state compared to cracking at internal C−C bonds. For all catalysts, measured activation entropies at the central C−C bond were comparable for both pathways, indicating the similarity between the two transition state structures.

Differences in apparent energies of activation correspond to enthalpic and entropic differences between the adsorbed molecules. For *n*-pentane, the heat of adsorption increases by 10 kJ/mol when going from H-USY (46 kJ/mol) to La-X (56 kJ/mol)[1,27] and the apparent activation energy for cracking drops by 16 kJ/mol and for dehydrogenation by 49 kJ/mol. This indicates a decrease in the intrinsic energetic barriers (not solely an adsorption effect) due to the polarization effect of isolated La^{3+} present in La-USY and in La-X. Entropies of adsorption decreased by 17 J/(mol K) when going from H-USY (−88 J/mol K) to La-X (−105 J/mol K).[1,27] Table 6 shows that apparent activation entropies for cracking differ by a comparable values among the different samples. Consequently, true activation entropies are similar for H-USY and La-X for the cracking pathways. The difference in measured activation entropies reflects only the entropic difference between the gas phase and the adsorbed state. A greater decrease of the true activation entropy was observed for the dehydrogenation pathway. Interaction of isolated La-X with C−H restricts strongly the vibrational and rotational freedom of *n*-pentane and lowers the enthalpic barrier.

4.3.3. Catalytic Cracking of 2,2,4 -TMP. The enhancement of specific catalytic rates was even more pronounced with larger molecules. With La-USY, the La^{3+} cations hardly influenced the catalytic cracking of 2,2,4-TMP compared to that of USY. This is consistent with the data from IR spectroscopy of adsorbed pyridine and ^{139}La NMR spectroscopy. The predominant stabilization of La^{3+} in the form of monomeric $[La(OH)_n]^{3-n}$ species limited the interaction of hydrocarbons with La^{3+}. Only the accessible La cations in La-X were able to significantly polarize the branched hydrocarbons and increase the rate of 2,2,4-TMP dehydrogenation. Isobutane was the major product formed under these reaction conditions indicating that the cracking of 2,2,4-TMP in the *β*-position yields isobutene followed by hydride transfer to generate the alkane. Thus, the initial activation produced two carbenium ions (Scheme 2, adapted from ref 28). The observed activation energy of 2,2,4-TMP cracking increased in the presence of La^{3+} from 35 via 43 to 62 kJ/mol (Table 7). Because the absolute values and their increase are similar to the heat of adsorption of isobutane on the respective zeolites,[1] it is suggested that a step closely associated with the desorption of the products is rate determining and thus represent intrinsic activation energies. The pre-exponential factor increased when normalized to the concentration of protons, so more entropy was generated in the release of the product, a compensating behavior often found in the thermodynamics of adsorption.

Scheme 2. Proposed Reaction Mechanism for the Catalytic Cracking of in-Situ Formed Iso-octanes in the Presence of Accessible La^{3+} Cations Inside the Supercages of Zeolite Catalysts

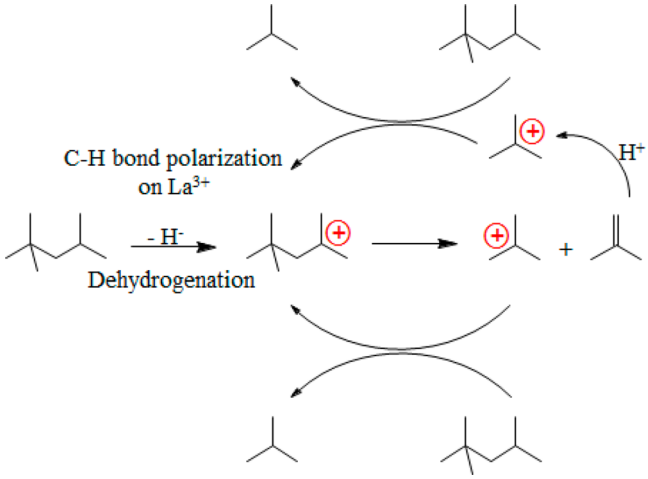

Adapted from ref 28. Copyright 2007 American Chemical Society.

5. CONCLUSIONS

H-USY, La-USY, and La-X catalysts with similar pore structures but different Si/Al ratios and La^{3+} concentrations were used to

dx.doi.org/10.1021/cs500200k | ACS Catal. 2014, 4, 1743−1752

study the impact of accessible La^{3+} for Brønsted acid catalyzed reactions. Overall, accessible La^{3+} polarizes C−H bonds in alkanes and stabilizes hydrides and hydride transfers. Less hydroxylated La^{3+} have stronger impact on catalysis.

The main role in cracking of propane and *n*-pentane of nonhydroxylated La^{3+} cations in La-X is to polarize C−H bonds resulting in enhanced dehydrogenation. This is supported by the unusually low energy of activation for dehydrogenation catalyzed by La-X. These variations in the energy of activation are related to the stronger polarization of the secondary C−H bond, with commensurate increase in the confinement of the transition states indicated by the greater entropy loss for alkane dehydrogenation on La-X.

Cracking of 2,2,4-trimethyl pentane shows that the polarization of the tertiary C−H bond and the subsequent dehydrogenation are not decisive for maintaining cracking activity at low temperatures. Increasing concentrations of La^{3+} led to higher rates. The low values of activation energies suggest that the rate determining step is not associated with the cleavage of the C−C bond but rather with the hydride transfer of the initially formed alkenes or the subsequent desorption.[29,30] The observed energies of activation are close to the heats of adsorption of isobutane in La-X suggesting that the observed activation energies are intrinsically linked to the product desorption.[1,10] The increase in the intrinsic energy of activation for the overall process is hence attributed to the stronger interaction of the products with the catalyst.

Finally, the drastic improvement of the catalytic activity for isobutane alkylation with 2-butene is a consequence of improved hydride transfer and of cracking induced by the presence of La^{3+}. This leads to a longer catalyst lifetime. Improved cracking and hydride transfer controlled the accretion of oligomers that eventually deactivate the catalyst by encapsulation. It is unclear whether the superior hydride transfer abilities are related to a greater polarization of the C−H bonds and hence a more active hydride transfer or whether the transition state itself is stabilized in a unique way.

The present study shows that accessible polarizable cations such as La^{3+} are able to generate a unique environment for hydrocarbon reactions. The fact that only La-X showed such enhanced catalytic properties emphasizes the importance of the coordination of La^{3+} and guides the development for new generations of catalysts.

AUTHOR INFORMATION

Corresponding Author

*E-mail: Johannes.lercher@ch.tum.de.

Present Address

[†]H.S.: Pacific Northwest National Laboratory, 902 Battelle Boulevard, P.O. Box 999, MSIN K2-57, Richland, WA 99352, USA.

Notes

The authors declare no competing financial interest.

ACKNOWLEDGMENTS

We thank Professor Cornelia Breitkopf for fruitful discussions regarding the network of IDECAT. Support of Dr. Gerhard Althoff with respect to the ^{139}La NMR measurements is gratefully acknowledged.

REFERENCES

(1) Sievers, C.; Onda, A.; Olindo, R.; Lercher, J. A. *J. Phys. Chem. C* **2007**, *111*, 5454−5464.
(2) Guzman, A.; Zuazo, I.; Feller, A.; Olindo, R.; Sievers, C.; Lercher, J. A. *Microporous Mesoporous Mater.* **2005**, *83*, 309−318.
(3) Venuto, P. B.; Hamilton, L. A.; Landis, P. S. *J. Catal.* **1966**, *5*, 484−493.
(4) Bolton, A. P. *J. Catal.* **1971**, *22*, 9−15.
(5) Feller, A.; Guzman, A.; Zuazo, I.; Lercher, J. A. *J. Catal.* **2004**, *224*, 80−93.
(6) Sievers, C.; Zuazo, I.; Guzman, A.; Olindo, R.; Syska, H.; Lercher, J. A. *J. Catal.* **2007**, *246*, 315−324.
(7) Flego, C.; Kiricsi, I.; Parker, W. O., Jr.; Clerici, M. G. *Appl. Catal., A* **1995**, *124*, 107−119.
(8) Diaz-Mendoza, F. A.; Pernett-Bolano, L.; Cardona-Martínez, N. *Thermochim. Acta* **1998**, *312*, 47−61.
(9) Sievers, C.; Liebert, J. S.; Stratmann, M. M.; Olindo, R.; Lercher, J. A. *Appl. Catal., A* **2008**, *336*, 89−100.
(10) Schüßler, F.; Pidko, E. A.; Kolvenbach, R.; Sievers, C.; Hensen, E. J. M.; van Santen, R. A.; Lercher, J. A. *J. Phys. Chem. C* **2011**, *115*, 21763−21776.
(11) Parry, E. P. *J. Catal.* **1963**, *2*, 371−379.
(12) Kunwar, A. C.; Turner, G. L.; Oldfield, E. *J. Magn. Reson.* **1986**, *69*, 124−127.
(13) Weihe, M.; Hunger, M.; Breuninger, M.; Karge, H. G.; Weitkamp, J. *J. Catal.* **2001**, *198*, 256−265.
(14) Herreros, B.; Man, P. P.; Manoli, J. M.; Fraissard, J. *J. Chem. Soc., Chem. Commun.* **1992**, 464−466.
(15) ASTM *Annual Book of ASTM Standards*; ASTM: West Conshohocken, PA, 1985; D3942-85.
(16) Feller, A.; Barth, J.-O.; Guzman, A.; Zuazo, I.; Lercher, J. A. *J. Catal.* **2003**, *220*, 192−206.
(17) Klein, H.; Fuess, H.; Hunger, M. *J. Chem. Soc., Faraday Trans.* **1995**, *91*, 1813−1824.
(18) Gaare, K.; Akporiaye, D. *J. Phys. Chem. B* **1997**, *101*, 48−54.
(19) Hunger, M.; Engelhardt, G.; Weitkamp. *J. Microporous Mater.* **1995**, *3*, 497−510.
(20) de Jong, K. P.; Mesters, C. M. A. M.; Peferoen, D. G. R.; van Brugge, P. T. M.; de Groot, C. *Chem. Eng. Sci.* **1996**, *51*, 2053−2060.
(21) Simpson, M. F.; Wei, J.; Sundaresan, S. *Ind. Eng. Chem. Res.* **1996**, *35*, 3861−3873.
(22) Feller, A.; Lercher, J. A. *Adv. Catal.* **2004**, *48*, 229−295.
(23) Gounder, R.; Iglesia, E. *J. Am. Chem. Soc.* **2009**, *131*, 1958−1971.
(24) Xu, B.; Bordiga, S.; Prins, R.; van Bokhoven, J. A. *Appl. Catal., A* **2007**, *333*, 245−253.
(25) Pidko, E. A.; van Santen, R. A.; Hensen, E. J. *Phys. Chem. Chem. Phys.* **2009**, *11*, 2893−2902.
(26) Narbeshuber, T. F.; Brait, A.; Seshan, K.; Lercher, J. A. *Appl. Catal., A* **1996**, *146*, 119−129.
(27) Eder, F.; Stockenhuber, M.; Lercher, J. A. *J. Phys. Chem. B* **1997**, *101*, 5414−5419.
(28) Sievers, C.; Onda, A.; Guzman, A.; Otillinger, K. S.; Olindo, R.; Lercher, J. A. *J. Phys. Chem. C* **2007**, *111*, 210−218.
(29) Blaszkowski, S. R.; Nascimento, M. A. C.; van Santen, R. A. *J. Phys. Chem.* **1996**, *100*, 3463−3472.
(30) Corma, A. *J. Catal.* **2003**, *216*, 298−312.